HHS Public Access

Author manuscript

Biofabrication. Author manuscript; available in PMC 2019 December 11.

Published in final edited form as:

Biofabrication. ; 12(1): 015008. doi:10.1088/1758-5090/ab48ca.

In situ tissue engineering of the tendon-to-bone interface by endogenous stem/progenitor cells

Solaiman Tarafder[1], **John A Brito**[1], **Sumeet Minhas**[1], **Linda Effiong**[2], **Stavros Thomopoulos**[2,3], **Chang H Lee**[1,4]

[1]Regenerative Engineering Laboratory, Columbia University Medical Center, 630 W. 168th Street, VC12-230, NY 10032, New York

[2]Department of Orthopedic Surgery, Columbia University Medical Center, 650 W. 168th Street, BB14-1408, NY 10032, New York

[3]Department of Biomedical Engineering, Columbia University, 351 Engineering Terrace, NY 10027, New York

Abstract

The long-term success of surgical repair of rotator cuff tears is largely dependent on restoration of a functional tendon-to-bone interface. We implemented micro-precise spatiotemporal delivery of growth factors in three-dimensional printed scaffolds for integrative regeneration of a fibrocartilaginous tendon-to-bone interface. Sustained and spatially controlled release of tenogenic, chondrogenic and osteogenic growth factors was achieved using microsphere-based delivery carriers embedded in thin membrane-like scaffolds. *In vitro,* the scaffolds embedded with spatiotemporal delivery of growth factors successfully guided regional differentiation of mesenchymal progenitor cells, forming multiphase tissues with tendon-like, cartilage-like and bone-like regions. *In vivo,* when implanted at the interface between the supraspinatus tendon and the humeral head in a rat rotator cuff repair model, these scaffolds promoted recruitment of endogenous tendon progenitor cells followed by integrative healing of tendon and bone via re-formation of strong fibrocartilaginous interfaces. Our findings demonstrate the potential of *in situ* tissue engineering of tendon-to-bone interfaces by endogenous progenitor cells. The *in situ* tissue engineering approach shows translational potential for improving outcomes after rotator cuff repair

Keywords

in situ tissue engineering; rotator cuff; controlled delivery; 3D printing embedded with spatiotemporal delivery

[4]Author to whom any correspondence should be addressed. chl2109@cumc.columbia.edu.

Author contributions

STa was responsible for primary technical undertaking and conducted the experiments, performed animal surgeries, collected and analyzed data, and drafted the manuscript. JAB contributed to the scaffold fabrication and cell culture. SM participated in animal surgeries. LE performed micro-CT analysis. STh contributed to the study design and micro-CT data interpretation. CHL was responsible for the study design, data interpretation and manuscript preparation. All the authors reviewed and edited the manuscript.

Supplementary material for this article is available online

Introduction

The rotator cuff of the shoulder is made up of four tendons inserting into the head of the humerus: the subscapularis, supraspinatus, infraspinatus and teres minor [1]. These tendons are susceptible to injury after excessive loading and/or degenerative tendinopathy, leading to structural and functional deterioration [1–4]. Clinically, rotator cuff injuries are the leading cause of shoulder pain and dysfunction and frequently require surgical intervention [4]. Each year in the United States, approximately 4.5 million patients visit physicians due to rotator cuff injuries and over 200 000 surgical repairs are performed [2].

Surgical repair of torn rotator cuff tendons requires reattachment of the tendon to its humeral head bony attachment, but current approaches have unacceptably low success rates [1–4]. Failure is probably due to a lack of functional re-integration of the injured tendon into its bony attachment, with formation of weak fibrovascular scar tissue at the interface [5–7]. The natural ten-don-to-bone attachment, also referred to as the enthesis, features a fibrocartilaginous interface with a gradient in structure and composition from tendon to bone: dense and highly aligned collagen fibrils in tendon, transitioning into unmineralized fibrocartilage, then mineralized fibrocartilage and then bone [8]. This complex functionally grsaded interface, with multiple integrated zones, is critical for minimizing stress concentrations and allowing for effective load transfer between tendon and bone [9]. In contrast, the fibrovascular scar tissue that forms during tendon-to-bone healing after surgical repair has inferior mechanical properties and results in high re-tear rates [5–7].

Various tissue engineering approaches have been investigated to improve healing of the tendon-to-bone interface, including formation of integrated fibrocartilage layers [10–18]. Natural or synthetic biomaterials, including poly(glycolic acid) (PGA), poly (lactic-co-glycolic acid) (PLGA) and polycarprolactone (PCL), either in mesh form or as nanofibrous membranes, have been applied in animal models of rotator cuff repair [3,4,19,20]. The biomaterial scaffolds were often delivered seeded with stem/progenitor cells and/or growth factors (GFs) to promote tendon-to-bone healing [21–23]. For example, nanofibrous scaffolds with gradients in mineral content were fabricated and tested for promotion of ten-don-to-bone interface regeneration both *in vitro* and *in vivo* [24, 25]. Mesenchymal stem cells (MSCs) or MSC-derived self-assembled tissue constructs have also been applied without any scaffold material, producing modest improvements in outcomes for ten-don-to-bone healing [19,20,26].

The above-mentioned previous works demonstrated the potential for integrated reconstruction of tendon-to-bone interfaces for rotator cuff repair. However, it remains challenging to achieve functional regeneration of a multi-tissue transition at the tendon-to-bone interface. Recently, we developed a micro-precise spatiotemporal delivery system embedded in three-dimensional (3D)-printed scaffolds, enabling the delivery of multiple GFs to desired locations with varied release rates [27,28] and high spatial resolution. These scaffolds showed great promise for engineering multi-tissue complexes by inducing regional differentiation of stem/progenitor cells [28]. In the current study, we applied this new platform for *in situ* engineering of a fibrocartilaginous matrix gradient at the supraspinatus tendon-to-bone interface by endogenous stem/progenitor cells. We hypothesized that

spatiotemporally released GFs from 3D-printed scaffolds will guide region-specific differentiation of endogenous mesenchymal stem/progenitor cells, consequently leading to regeneration of a functional tendon-to-bone attachment *in vivo*. After confirming multi-tissue formation by regional differentiation of MSCs *in vitro*, the GF-embedded scaffolds were tested in an established rat model of rotator cuff repair. Given the significant translational barriers to cell transplantation [29–31], here we adopted the emerging '*in situ* tissue engineering' approach by harnessing endogenous tendon stem/progenitor cells, as demonstrated in our recent work [27,28].

Methods

Design and fabrication of 3D-printed scaffolds with spatiotemporal delivery of multiple growth factors

To recapitulate the gradient matrix distribution at the native tendon-to-bone interface, an integrated, three-layered 3D scaffold was fabricated by 3D printing with spatiotemporal delivery of multiple GFs (figure 1(a)). For sustained release, connective tissue growth factor (CTGF), transforming growth factor beta 3 (TGF, β3) and bone morphogenetic protein 2 (BMP2) were encapsulated in PLGA microspheres (μS) by a double-emulsion technique as per our established methods [27, 32]. CTGF-and BMP2-encapsulated μS were printed as embedded in PCL microstrands on the top and bottom layers for tendon and bone regions, respectively (figure 1(a)). CTGF-and TGFβ3-μS embedded in PCL were printed on the middle layer for the fibrocartilage interface layer between tendon and bone (figure 1(a)). All 3D printing processes were performed with a 3D Bioplotter® (EnvisionTec, Germany) as per our previous work [27,28]. A distance of 300–400, μm was applied between microstrands and a strand diameter of 200–400 μm was maintained during printing. Scaffolds for the control group without GF were printed with the same design and printing parameters, embedding empty μS into the PCL microstrands (−GF). Both control (−GF) and GF-loaded scaffolds were treated with 6 M NaOH for 4 h to introduce surface micro-pores for accelerated release of the GFs, as in our previous work [28]. The scaffold was designed to be implanted between the supraspinatus tendon and the bone of the humerus in surgically repaired rat rotator cuffs (figure 1(b)). Three-layered scaffolds had porous structures, allowing for cell infiltration (figure 1(c)) and material flexibility to fit onto the anatomical contour of the humeral head (figure 1(d)).

In vitro engineering of the fibrocartilaginous matrix gradient interface with human MSCs

Human MSCs were cultured in the three-layered 3D-printed scaffolds following our established protocol [27, 28, 31, 32]. Briefly, passage 3–4 MSCs (adult donor, obtained from All Cells, Alameda, CA, USA) were reconstituted in neutralized collagen type I (COL-I; 2mgmL^{-1}) solution at a final density of 2 million cells mL^{-1}. Then, MSC-loaded COL-I solution (50, μL) was applied to the 3D-printed PCL scaffolds (5 mm × 3 mm × 1 mm) embedded with either GF-, μS or empty μS, followed by incubation for 30 min at 37 °C for collagen cross-linking. A 1:1:1 mixture of fibrogenic induction supplement (50 μg mL^{-1} ascorbic acid), chondrogenic induction supplement (1% 1X insulin-transferrin-selenium (ITS) + 1 solution, 10 mM sodium pyruvate, 50 μg mL^{-1} L-ascorbic acid 2-phosphate, 40 μg mL^{-1} L-proline and 0.1 μM dex-amethasone) and osteogenic induction supplement (10 mM

β-glycerophosphate) were applied, and the medium was changed every other day for 6 weeks.

Total collagen assay, glycosaminoglycan (GAG) content assay and biomechanical tests were performed on the samples after 6 weeks' culture. Briefly, total soluble collagen and GAG content assays were carried out using a Sircol™ soluble collagen assay kit (Biocolor Ltd, Carrickfergus, UK) and a Blyscan™ sulfated GAG assay kit (Biocolor Ltd, Carrickfergus, UK), respectively. Tensile moduli of 3D-printed rotator cuff scaffolds after 6 weeks' culture with MSCs were evaluated using a BioDynamics testing system (TA Instruments, New Castle, DE, USA) as per our prior method [27,29, 31]. Briefly, tensile tests were performed at 1% strain/min after preconditioning for 15 cycles (0%–10% strain), followed by measuring the tensile modulus from the linear region of each stress-strain curve. For histology and immunohistochemical analyses, scaffolds were fixed in 10% formalin followed by embedding in paraffin after harvesting. Immunofluorescence imaging was performed for COL-I and COL-II, aggrecan and osteocalcin (OC) as per our prior methods [31].

In vivo healing of the tendon-to-bone fibrocartilaginous interface

All animal procedures were approved by the Institutional Animal Care and Use Committee at Columbia University, NY, USA. Twelve-week-old Sprague-Dawley rats were placed in an induction chamber with isoflurane administration at 1% 20135% for induction of anesthesia; the rats were then placed on a surgical table. Continuous isoflurane administration at 1% – 3% was used for maintenance of anesthesia. The anesthetic state were checked using hind limb toe pinch and respiratory observation. Sustained release buprenorphine was administrated prior to surgery. The surgical site was shaved, prepped with povidone iodine/ethanol and draped in a sterile surgical manner followed by administration of local anesthetic (2% lidocaine with 1:200 000 epinephrine). The surgery and the implantation were performed using a method slightly modified from the well-established procedure for tendon detachment and reattachment [14, 22, 33]. Briefly, a longitudinal anterolateral skin incision was made on left shoulder to partially detach deltoid muscle from the posterolateral section of the acromion and then split distally from the anterolateral corner of the acromion. The supraspinatus tendon was identified and transected sharply at its insertion on the greater tuberosity using a scalpel blade. A dental bur was used to decorticate the tuberosity, followed by debriding of all soft tissue and fibrocartilage at the surgical site. Then a scaffold of dimensions 3 mm × 5 mm × 0.5 mm (width × length × thickness) was secured to the tendon with a no. 5 nylon suture with the layer with embedded CTGF μS facing the tendon. The suture ends from the tendon were passed through a 1.0 mm bone tunnel created at the anterior and posterior portions of the insertion site and tied over the humeral cortex to ensure re-approximation of the repaired tendon to the bone, where the scaffold was secured between tendon and bone. The surgical site was then closed using 4–0 absorbable sutures for the subcutaneous layer and 4–0 nylon sutures for skin closure. After complete recovery from anesthesia, rats were placed in cages and allowed to resume a normal diet. A total of 22 rats (n = 11 per group) were used and sacrificed after either 1 or 4 weeks of healing. The harvested tissues were wrapped in a gauze pre-wetted with saline and kept at –20 °C until mechanical analysis (total n = 8 per group) or fixed in formalin for histology and

immunohistochemical analyses (total $n = 3$ per group). The trabecular bone of the humeral head at the repair site ($n = 3$ per group) was analyzed using microcomputed tomography (micro-CT) (SCANCO mCT40) with 20 mm resolution and 300 ms integration time at 45 kV/177 mA as per the established protocol [24].

Collagen fiber organization

Automated digital imaging processing was used to quantify the angular frequency of collagen fibers in tendons as per our established methods [30]. Briefly, Picrosirius red (PR) staining and polarized light microscopy were used to analyze the collagen fiber organization at the supraspinatus tendon attachment sites. Circularly polarized images (six images per group) were obtained and underwent 8-bit digitization with ImageJ at a resolution of 1360 × 1024 pixels. An in-house written MATLAB code was used for automated imaging processing for measuring the angular frequency of collagen fibers, and the angular deviation (AD) was calculated as the average of the standard deviations of the angular frequencies [30].

Biomechanical evaluation

The mechanical properties of the harvested tendon-to-bone interfaces were measured using a BioDynamics testing system (TA Instruments, New Castle, DE, USA) as per previously reported procedures [3, 27, 34, 35]. Briefly, the harvested shoulder specimens ($n = 8$ per group) were wrapped in gauze, wetted with physiological saline solution, kept in a Ziploc bag and stored at –20 °C until biomechanical testing. Specimens were thawed at room temperature on the day of testing, and surrounding tissues were carefully removed from the dissected humerus-tendon complexes. The humerus was positioned in a custom-designed grip that prevents fracture through the humeral physis, and the free end of the supraspinatus tendon was secured in a tension grip to prevent any slipping during testing. Tensile tests were done at 5% strain/min after preconditioning for 10 cycles (0% – 5% strain) at a frequency of 0.5 Hz. Saline spray was used to keep the specimen moist throughout testing. The maximum load at tensile failure and stiffness were determined from the load-displacement plots following a well-established protocol [14,33].

Statistics

Sample sizes for all quantitative data were determined by power analysis using an α level of 0.05, power of 0.8 and effect size of 1.50 to assess matrix synthesis, angular deviations and mechanical properties in the regenerated tendon-to-bone interface upon verification of normal data distribution. For all quantitative data, one-way analysis of variance with post-hoc Tukey honestly significant difference tests were used. All data are presented as the mean ± standard deviation.

Results

Engineered fibrocartilaginous matrix gradient *in vitro*

Reconstruction of an integrated fibrocartilaginous matrix gradient remains one of the biggest challenges for regeneration of the tendon-to-bone interface. Here, we constructed 3D-printed, three-layered scaffolds with spatially delivered CTGF, CTGF + TGFβ3, and BMP2

via embedded PLGA μS (figure 1(a)) for regenerating a fibrocartilaginous matrix gradient by regulating the spatial differentiation of MSCs. The GFs were selected on the basis of recent works from our group and others, which showed CTGF to be a potent tenogenic cue [31, 36] and a combination of CTGF and TGFβ3 as an inducer for fibrocartilaginous differentiation of MSCs from various sources [31]. The role of BMP2 in osteogenic differentiation of MSCs has been well described [37]. When cultured with human MSCs for 6 weeks, the scaffolds with spatiotemporally delivered GFs (+GF) showed an abundant COL-I^{+} matrix compared with the control group with empty μS (−GF) (figure 2(a)). COL-II^{+} and GAG^{+} fibrocartilaginous matrices were formed in the middle zone of +GF scaffolds, distinct from the −GF control (figure 2(a)). OC expression was observed on the BMP2-delivered bone layer in the +GF scaffolds, in comparison with minimal OC expression in the −GF group (figure 2(a)). Quantitatively, +GF scaffolds cultured with MSCs for 6 weeks resulted in significantly higher collagen and GAG contents than the −GF scaffolds (figure 2(b) and (c)) ($p < 0.0001$; $n = 6$ per group). Consistently, +GF scaffolds exhibited a significantly higher tensile modulus than did −GF scaffolds (figure 2(d)) ($p < 0.0001$; $n = 6$ per group). These findings collectively suggest the potential of our scaffold system for interface regeneration within a multi-tissue complex by guiding regional differentiation of MSCs.

In situ regeneration of supraspinatus tendon-to-bone insertion with a native-like fibrocartilaginous matrix gradient interface

Acellular scaffolds were implanted at the interface between tendon and bone in the rat supraspinatus tendon repair model (figure 3(a)). Tissue samples harvested 4 weeks post-operatively from both −GF and +GF groups showed no sign of visible inflammation (figure 3(a)), suggesting that PLGA μS embedded PCL scaffolds and their degradation by-products were well tolerated at the tissue level. Histological sections with PR staining showed the formation of collagen-rich tissue at the tendon-to-bone interface in both −GF and +GF groups (figure 3(b)). Notably, the +GF group had a well-organized collagen structure, reminiscent of the native interface, whereas a scar-like disrupted fibrous interface was formed in the −GF group (figure 3(b)). A proteoglycan/GAG-rich fibrocartilaginous matrix interface similar to the native interface was also reconstructed in the +GF group, as evidenced by Alcian blue (AB) staining, in contrast to the disrupted matrix which lacked proteoglycan/GAG in the −GF group (figure 3(c)). The appearance of rounded fibrochondrocyte-like cells and mineralized fibrocartilage at the tendon-to-bone insertion site in the +GF group suggested that spatiotemporal delivery of the specific GFs through the tissue engineered scaffolds promoted regeneration of a fibrocartilaginous matrix gradient interface at the repaired supraspinatus tendon-to-bone insertion site. Consistently, the +GF group showed a native-like COL-II^{+} fibrocartilaginous matrix gradient, while a fibrous scar formed at the interface in the −GF group demonstrated a lack of COL-II expression (figure 3(d)).

Alignment of collagen fibers at the *in situ* engineered tendon-to-bone interface

In native tendon-to-bone interfaces, highly aligned collagen fibers from tendon are interdigitated into the mineralized fibrocartilage passing through the unmineralized fibrocartilage region (figures 3(b)–(d)). Four weeks post-operatively, circularly polarized

microscopy images with PR staining revealed densely aligned tendon collagen fibers at the tendon-to-bone insertion site with +GF scaffolds, whereas a disorganized collagen structure was seen with 2014 GF scaffolds (figure 4(a)). As per the automated digital image processing, a native-like, narrow angular distribution of collagen fibers was seen in the +GF group compared with a broad distribution in the −GF group (figure 4(b)). Quantitatively, the tendon-to-bone interface with +GF scaffolds exhibited an AD of the collagen fibers across the interface similar to the native one, while −GF scaffolds exhibited a significantly higher AD than the native and +GF values (figure 4(c)).

Tensile properties and bone healing

Consistent with the above-described histological and image-analysis data, the tendon-to-bone interfaces with +GF scaffolds had a significantly higher tensile maximum load and stiffness (figure 5(a)) than the samples with −GF scaffolds ($p < 0.01$; $n = 8$ per group). Micro-CT analysis further demonstrated that the +GF group had a higher bone volume than the −GF group (figures 5(b)–(d)). Compared with unimplanted PCL scaffolds embedded with μS, +GF scaffolds showed significantly higher tensile stiffness and maximum load, whereas −GF scaffolds showed lower tensile properties (supplementary figure 1(a), available online at stacks.iop.org/BF/12/015008/mmedia)($p < 0.05$; $n = 4$ per group), suggesting that the improved tensile properties may be attributed to newly formed tissues. In addition, +GF group showed a toe region in the load versus displacement curve similar to the native one, whereas the −GF group did not show a toe region (supplementary figure 1 (b)).

Endogenous cell source for tendon-to-bone interface healing

Tissue samples were harvested 1 week post-operatively to determine the potential source of the endogenous cells responsible for *in vivo* healing of tendon-to-bone interfaces by the GF-embedded scaffolds. Remnants of the scaffold structures remained at this timepoint (voids marked as * in figure 6) and infiltrated with host cells in both the +GF and −GF groups (figures 6(a)–(e) and (f)–(j)). Immunofluorescence demonstrated that more $CD146^+$ tendon stem/progenitor-like cells were present in +GF scaffolds than in −GF scaffolds (figures 6(a)–(e) and (f)–(j)). In addition, $CD146^+$ tendon stem/progenitor cells appeared to originate from the tendon and not from the bone (figure 6(a)–(e)).

Discussion

The present findings demonstrate the potential of *in situ* tissue engineering approaches for regeneration of the tendon-to-bone interface by endogenous stem/progenitor cells. Our micro-precise spatiotemporal delivery system embedded in 3D-printed flexible scaffolds enabled engineering of an integrated multiphase tendon-to-bone interface both *in vitro* and *in vivo.* Given that no cells were delivered with the scaffolds *in vivo*, endogenous cells were solely responsible for healing the tendon-to-bone interface. CD146 is a pericyte marker and was recently identified as a marker for highly regenerative tendon-resident stem/progenitor cells [30, 38]. $CD146^+$ tendon stem/progenitor cells are multipotent, highly clonogenic and pivotal in CTGF-induced tendon regeneration [30]. The immunofluorescence analysis in the current study revealed infiltration and possible expansion of $CD146^+$ cells into the GF-embedded scaffolds 1 week post-operatively, suggesting an endogenous cell source for

tendon-to-bone interface healing. Thus, GFs released by these scaffolds, including chemotactic/profibrogenic CTGF, may have increased the number of $CD146^+$ tendon stem/progenitor cells, leading to improved tendon-to-bone interface healing, consistent with our previous study using this GF for articular cartilage repair [30].

Despite the identification of $CD146^+$ cells in the early phase of healing, the *in vivo* fate of these cells in the later phases of tendon-to-bone interface healing is not known. In vivo tracing of specific stem/progenitor cell populations is now feasible using reporter mouse lines with tissue-specific green or red fluorescent protein labeling [39–42]. However, the mouse rotator cuff is too small to perform the surgical procedure and implant scaffolds. Given the paucity of lineage-tracing tools in a rat model, it remains technically challenging to investigate the specific roles and fates of the endogenous $CD146^+$ tendon stem/progenitor cells at the healing tendon-to-bone interface. Further advancement in genetic rat models and/or *in vivo* cell tracing technology will potentially provide a better understanding of the specific roles of endogenous cells in healing of tendon-to-bone interfaces.

Previous studies using lineage-tracing mouse models identified several markers important for enthesis development and maturation, including Scx, Sox-9, Glil and GDF5 [39–41]. Hedgehog-active $GDF5^+$ and $Gli1^+$ cells, distinct from tenocytes and epiphyseal chondrocytes, appeared to be the progenitor cells for formation of mineralized fibrocartilage in tendon-to-bone interfaces [39–41]. These enthesis progenitor cells are initially located at the interface between the epiphyseal cartilage and the tendon [39–41], which may not be distinct from $CD146^+$ tendon stem/progenitor cells. In addition, a recent study demonstrated that the $Gli1^+$ progenitor cells exhibit the capacity to heal immature enthesis after injury but not the mature tendon enthesis [40]. Accordingly, it is unclear if the populations of endogenous cells and the key signaling cues leading to healing of the tendon-to-bone interface differ between premature and mature tissues. A follow-up lineage-tracing study may be necessary to understand any potential link(s) between the early progenitor cells (e.g. Scx^+, $Sox\text{-}9^+$, $GDF5^+$ and/or $Gli1^+$) and the later $CD146^+$ stem/progenitor cells in adult tendon entheses.

Although our GF-embedded 3D-printed scaffolds resulted in a statistically significant improvement in the mechanical properties of the tendon-to-bone interface, the outcome remained significantly below the native levels after 4 weeks of healing. This result is probably due to the immaturity of the newly formed collagen matrix at the 4 week timepoint [43]. A follow-up study will be necessary to determine the long-term functional outcomes in tendon-to-bone interface healing by GF-embedded 3D-printed scaffolds and endogenous stem/progenitor cells. Our ongoing work also includes further optimization of the doses and release rates of the GFs. Compared with the direct application of GFs subjected to quick diffusion *in vivo,* controlled delivery providing sustained release improves healing or engineering of various musculoskeletal tissues [27, 28, 31, 36, 44, 45]. In this study, we adopted the doses and release kinetics that were pre-optimized from our previous works for regeneration of fibrocartilaginous tissues in small animals [28]. However, further refined control of doses and release rates will be conducted in our follow-up studies, given our recent findings suggesting that the duration and/or release rate of bioactive cues may be attributed to the quality of tissue healing, depending upon the type of tissue [27,44].

In conclusion, we successfully engineered multiphase fibrocartilaginous tendon-to-bone interfaces using endogenous stem/progenitor cells. Sustained-released of GFs from 3D-printed scaffolds successfully promoted the recruitment of endogenous stem/progenitor cells and their regional differentiation, consequently leading to enhanced healing of tendon-to-bone interfaces. Given that this approach does not require cell isolation, culture/expansion and manipulation of cells *in vitro,* the scaffolds embedded with micro-precise spatiotemporal delivery of GFs have potential as off-the-shelf graft products available for patients undergoing rotator cuff repair surgery.

Supplementary Material

Refer to Web version on PubMed Central for supplementary material.

Acknowledgments

We thank Abrar Nadroo and Richard Clough for their assistance with the *in vitro* cell culture experiments. NIAMS R01AR071316-03 and NIDCR R03DE026794-02 in part supported this study.

References

[1]. Depres-Tremblay G, Chevrier A, Snow M, Hurtig MB, Rodeo S and Buschmann MD 2016 Rotator cuff repair: a review of surgical techniques, animal models, and new technologies under development J. Shoulder Elbow Surg 25 2078–85 [PubMed: 27554609]

[2]. Mather RC III et al.2013 The societal and economic value of rotator cuff repair J. Bone Joint Surg. Am 95 1993–2000 [PubMed: 24257656]

[3]. Yokoya S, Mochizuki Y, Nagata Y, Deie M and Ochi M2008 Tendon-bone insertion repair and regeneration using polyglycolic acid sheet in the rabbit rotator cuff injury model Am. J. Sports Med 36 1298–309 [PubMed: 18354143]

[4]. Yokoya S, Mochizuki Y, Natsu K, Omae H, Nagata Y and Ochi M 2012 Rotator cuff regeneration using a bioabsorbable material with bone marrow-derived mesenchymal stem cells in a rabbit model Am. J. Sports Med 40 1259–68 [PubMed: 22491821]

[5]. Bishop J, Klepps S, Lo IK, Bird J, Gladstone JN and Flatow EL 2006 Cuff integrity after arthroscopic versus open rotator cuff repair: a prospective study J. Shoulder Elbow Surg 15 290–9 [PubMed: 16679227]

[6]. Verma NN et al. 2006All-arthroscopic versus mini-open rotator cuff repair: a retrospective review with minimum 2-year follow-up Arthroscopy 22 587–94 [PubMed: 16762695]

[7]. Gasbarro G et al. 2016 Morphologic risk factors in predicting symptomatic structural failure of arthroscopic rotator cuff repairs: tear size, location, and atrophy matter Arthroscopy. 32 1947–52 [PubMed: 27129377]

[8]. Killian ML and Thomopoulos S 2016 Scleraxis is required for the development of a functional tendon enthesis FASEB J. 30 301–11 [PubMed: 26443819]

[9]. Deymier-Black AC, Pasteris JD, Genin GM and Thomopoulos S 2015 Allometry of the tendon enthesis: mechanisms of load transfer between tendon and bone J. Biomech. Eng 137111005

[10]. Sun YY et al. 2016 A synthetic bridging patch of modified coelectrospun dual nano-scaffolds for massive rotator cuff tear J. Mater. Chem B 4 7259–69

[11]. Zheng Z et al. 2017Alignment of collagen fiber in knitted silk scaffold for functional massive rotator cuff repair Acta Biomater. 51 317–29 [PubMed: 28093363]

[12]. Suh DS et al. 2017 Atelocollagen enhances the healing of rotator cuff tendon in rabbit model Am. J. Sports Med 45 2019–2027 [PubMed: 28586622]

[13]. Tokunaga T. et al. 2017; Enhancement of rotator cuff tendon-bone healing with fibroblast growth factor 2 impregnated in gelatin hydrogel sheets in a rabbit model. J. Shoulder Elbow Surg. 26

[14]. Kovacevic D, Gulotta LV, Ying L, Ehteshami JR, Deng XH and Rodeo SA2015 rhPDGF-BB promotes early healing in a rat rotator cuff repair model Clin. Orthop. Relat. Res 473 1644–54 [PubMed: 25349036]

[15]. Pan J et al. 2015 Rotator cuff repair using ac decellularized tendon slices graft: an in vivo study in a rabbit model Knee Surg. Sports Traumatol. Arthroscopy 23 1524–35

[16]. Ji XX et al. 2015 Rotator cuff repair with a tendon-fibrocartilage-bone composite bridging patch Clin. Biomech 30 976–80

[17]. Smith MJ et al. 2012 Comparison of a novel bone-tendon allograft with a human dermis-derived patch for repair of chronic large rotator cuff tears using a canine model Arthroscopy 28 169–77 [PubMed: 22137238]

[18]. Beason DPet al. 2012 Fiber-aligned polymer scaffolds for rotator cuff repair in a ratmodel J. Shoulder Elbow Surg 21245–50

[19]. Degen RM et al. 2016 The effect of purified human bone marrow-derived mesenchymal stem cells on rotator cuff tendon healing in an athymic rat Arthroscopy32 2435–43 [PubMed: 27282111]

[20]. Novakova SS et al. 2018 Tissue-engineered tendon constructs for rotator cuff repair in sheep J. Orthop. Res 36 289–99 [PubMed: 28657154]

[21]. Huegel J et al. 2017 Autologous tendon-derived cell-seeded nanofibrous scaffolds improve rotator cuff repair in an age-dependent fashion J. Orthop. Res 35 1250–7 [PubMed: 27500782]

[22]. Omi R, Gingery A, Steinmann S P, Amadio PC, An KN and Zhao C 2016 Rotator cuff repair augmentation in a rat model that combines a multilayer xenograft tendon scaffold with bone marrow stromal cells J. Shoulder Elbow Surg 25 469–77 [PubMed: 26387915]

[23]. Peach MS. et al. 2017; Engineered stem cell niche matrices for rotator cuff tendon regenerative engineering. PLoS One. 12

[24]. Lipner J et al. 2015 In vivo evaluation of adipose-derived stromal cells delivered with a nanofiber scaffold for tendon-to-bone repair Tissue Eng. A21 2766–74

[25]. Moffat KL, Kwei AS, Spalazzi JP, Doty SB, Levine WN and Lu HH 2009 Novel nanofiber-based scaffold for rotator cuff repair and augmentation Tissue Eng. A15 115–26

[26]. Smietana MJ, Moncada-Larrotiz P, Arruda EM, Bedi A and Larkin LM 2017 Tissue-engineered tendon for enthesis regeneration in a rat rotator cuff model Biores. Open Access 6 47–57 [PubMed: 28736687]

[27]. Legemate K, Tarafder S, Jun Y and Lee CH2016 Engineering human TMJ discs with protein-releasing 3D-printed scaffolds J. Dent. Res 95 800–7 [PubMed: 27053116]

[28]. Tarafder S, Koch A,Jun Y, Chou C, Awadallah MR and Lee CH2016 Micro-precise spatiotemporal delivery system embedded in 3D printing for complex tissue regeneration Biofabrication 8 025003

[29]. Lee CH, Cook JL, Mendelson A, Moioli EK,Yao H and Mao JJ 2010 Regeneration of the articular surface of the rabbit synovial joint by cell homing: a proof of concept study Lancet376 440–8 [PubMed: 20692530]

[30]. Lee CH et al. 2015 Harnessing endogenous stem/progenitor cells for tendon regeneration J. Clin. Invest 125 2690–701 [PubMed: 26053662]

[31]. Lee CH, Rodeo SA, Fortier LA, Lu C, Erisken C and Mao JJ 2014 Protein-releasing polymeric scaffolds induce fibrochondrocytic differentiation of endogenous cells for knee meniscus regeneration in sheep Sci Transí. Med 6 266ra171

[32]. Lee CH, Marion NW, Hollister S and Mao JJ 2009 Tissue formation and vascularization in anatomically shaped human joint condyle ectopicallyin vivo Tissue Eng. A15 3923–30

[33]. Thomopoulos S et al. 2002 The localized expression of extracellular matrix components in healing tendon insertion sites: an in situ hybridization studyJ. Orthop. Res 20 454–63 [PubMed: 12038618]

[34]. Bedi A et al. 2010The effect of matrix metalloproteinase inhibition on tendon-to-bone healing in a rotator cuff repair model J. Shoulder Elbow Surg 19 384–91 [PubMed: 19800260]

[35]. Gimbel JA,Van Kleunen JP, Lake SP, Williams GR and Soslowsky LJ 2007 The role of repair tension on tendon to bone healing in an animal model of chronic rotator cuff tears J. Biomech 40 561–8 [PubMed: 16600252]

[36]. Lee CH, Shah B, Moioli EK and Mao JJ 2010 CTGF directs fibroblast differentiation from human mesenchymal stem/stromal cells and defines connective tissue healing in a rodent injury model J. Clin. Invest 120 3340–9 [PubMed: 20679726]

[37]. Ryoo HM, Lee MH and Kim YJ 2006 Critical molecular switches involved in BMP-2-induced osteogenic differentiation of mesenchymal cells Gene. 366 51–7 [PubMed: 16314053]

[38]. Yin Z. et al. 2016; Single-cell analysis reveals a nestin+ tendon stem/progenitor cell population with strong tenogenic potentiality. Sci. Adv. 2

[39]. Dyment NA et al. 2015 Gdf5 progenitors give rise to fibrocartilage cells that mineralize via hedgehog signaling to form the zonal enthesis Dev. Biol 405 96–107 [PubMed: 26141957]

[40]. Schwartz AG, Galatz LM and Thomopoulos S 2017 Enthesis regeneration: a role for Gli1+ progenitor cells Development 1441159–64

[41]. Schwartz AG, Long F and Thomopoulos S 2015 Enthesis fibrocartilage cells originate from a population of Hedgehog-responsive cells modulated by the loading environment Development 142 196–206 [PubMed: 25516975]

[42]. Yoshimoto Y, Takimoto A, Watanabe H, Hiraki Y, Kondoh G and Shukunami C2017 Scleraxis is required for maturation of tissue domains for proper integration of the musculoskeletal system Sci. Rep 7 45010

[43]. Kanazawa T. et al. 2016; Histomorphometric and ultrastructural analysis of the tendon-bone interface after rotator cuff repair in a rat model. Sci. Rep. 6

[44]. Tarafder S et al. 2019 Effect of dose and release rate of CTGF and TGFbeta3 on avascular meniscus healing J. Orthop. Res 37 1555–62 [PubMed: 30908692]

[45]. Tarafder S,Gulko J,Sim KH,Yang J,Cook JLandLee CH 2018 Engineered healing of avascular meniscus tears by stem cell recruitment Sci. Rep 8 8150 [PubMed: 29802356]

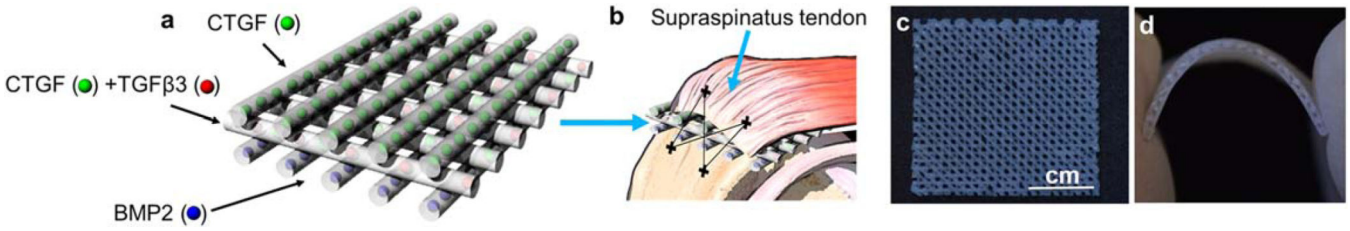

Figure 1.

Design of 3D-printed scaffolds with spatiotemporal deliveryof CTGF, TGFβ3 and BMP2 for regeneration of the rotator cuff tendon-to-bone interface with an integrated fibrocartilaginous matrix gradient. The scaffold consisted of three layers, with CTGF-encapsulated PLGA μS embedded in PCL microstrands at the top layer for tendon formation, CTGF μS and TGFβ3 μS embedded in the middle layer for fibrocartilage formation and BMP2 μS embedded in the bottom layer for bone formation (a). These scaffolds were designed to be implanted between tendon and bone along with surgical repair of the rat rotator cuff (b). The 3D-printed, GF-embedded three-layered PCL scaffolds were prepared as sheets (c) with high flexibility to fit to anatomical contour of humeral heads (d).

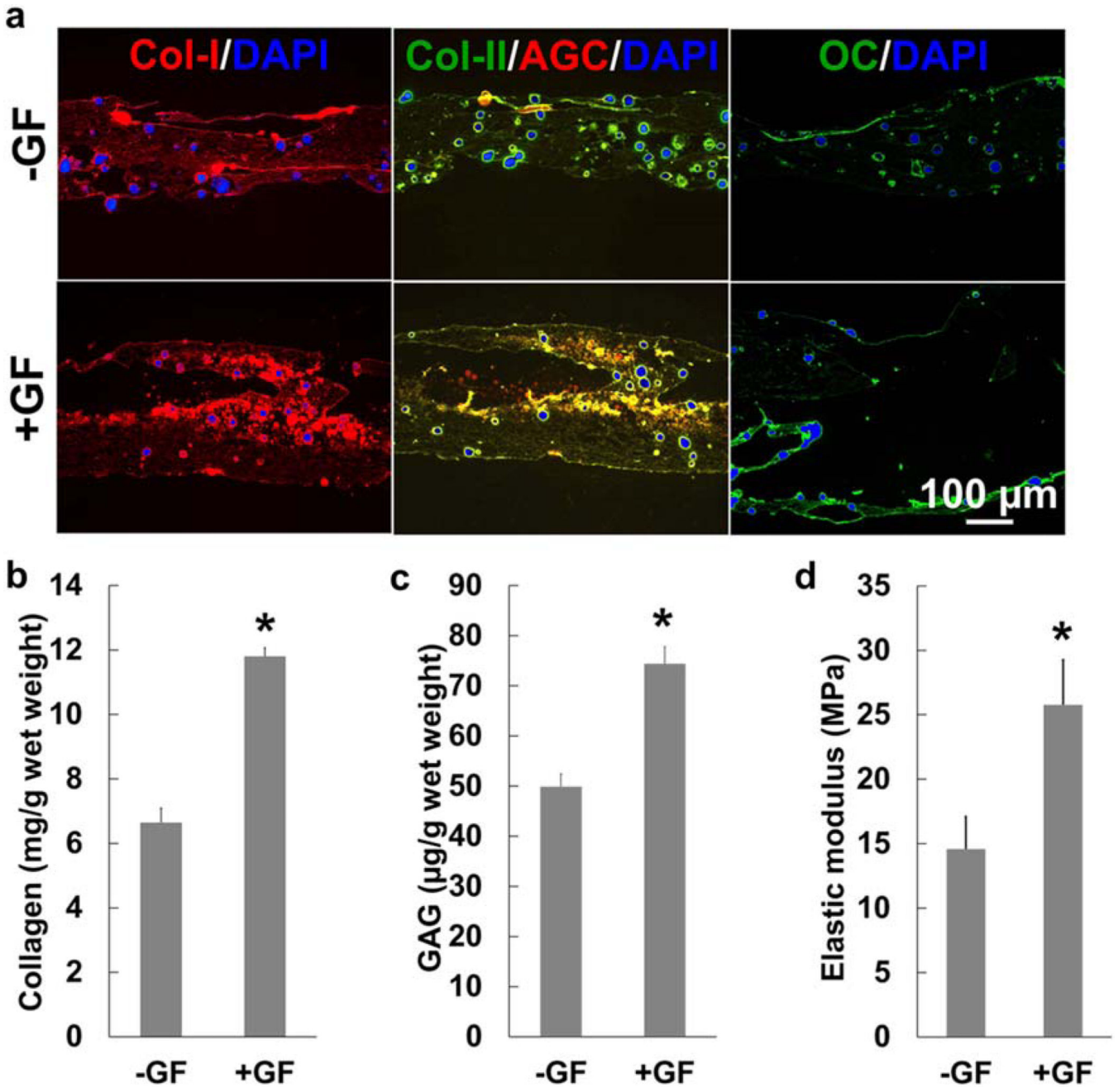

Figure 2.

Rotator cuff scaffolds embedded in a spatiotemporal delivery system guide the differentiation of human mesenchymal stem/progenitor cells (hMSCs) to form fibrocartilaginous matrix gradient tissue with a higher tensile modulus. After 6 weeks of culture with hMSCs, scaffolds with GF-μS(+GF) exhibited more Col-I rich matrix on the top and middle layers (a) compared with scaffolds with empty μS(−GF) (a) (DAPI, 4’,6-diamidino-2-phenylindole). Similarly, COL-II and GAG-rich matrices were notablyhigher in +GF than −GF, and OC expression was more abundant in the BMP2 layer in +GF in comparison with −GF (a). Quantitatively, +GF scaffolds induced significantlyhigher total

collagen (b) and GAG (c) contents. These changes to composition of the extracellular matrix led to increased tensile moduli of the +GF scaffolds compared with the −GF scaffolds (d) (*$p < 0.05$ compared with −GF; $n = 3$ per group; error bars indicate the standard deviation).

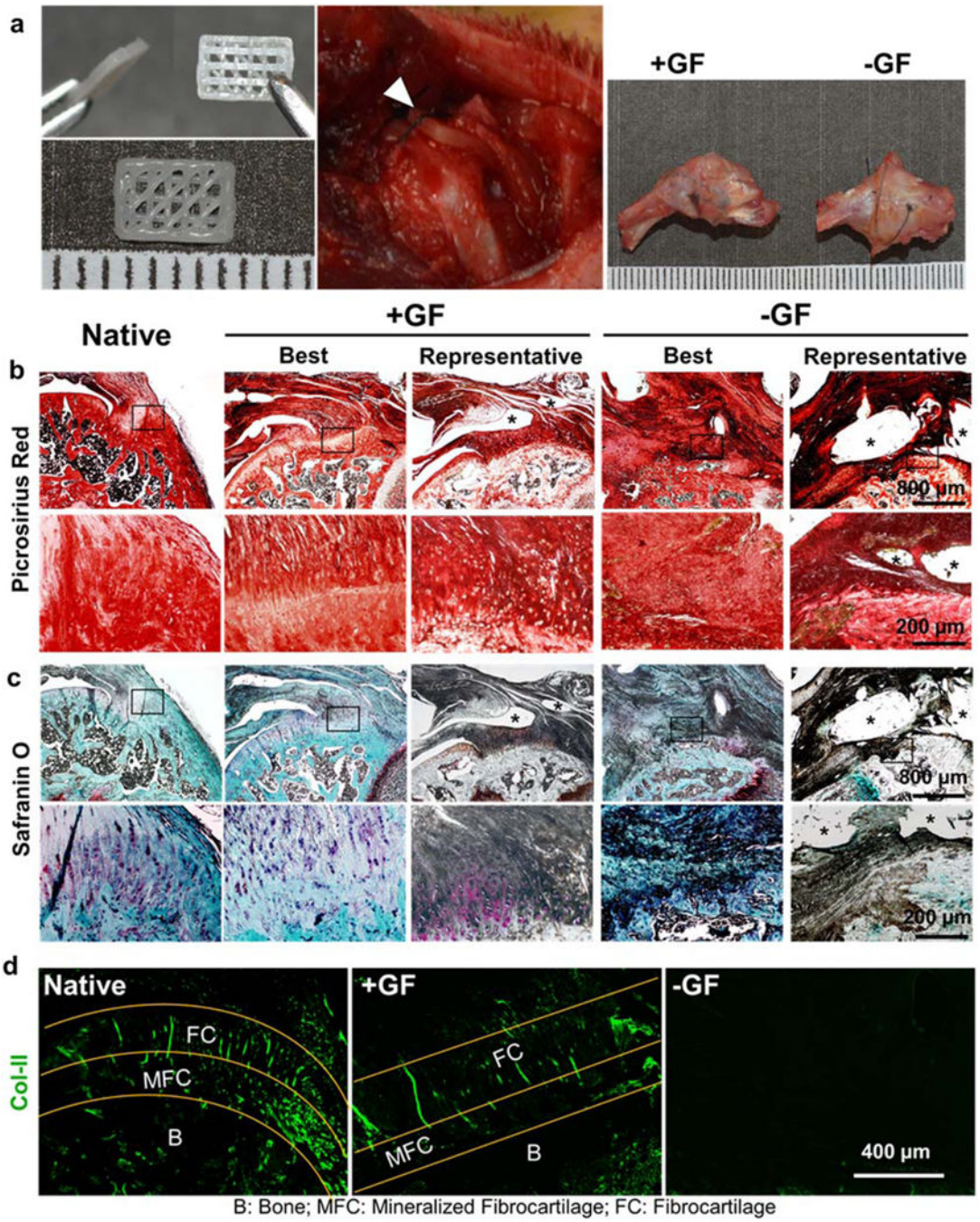

Figure 3.

Spatiotemporal deliveryof GFs via 3D-printed PCL scaffolds improved healing of the tendon-to-bone fibrocartilaginous interface *in vivo*. Three-layered scaffolds with spatially embedded GF-μS(+GF) or empty μS (−GF) were implanted between tendon and bone at the supraspinatus tendon-to-bone insertion site and tissue samples were harvested 4 weeks post-operatively (a). Grossly, the harvested tissues showed no noticeable difference between +GF and −GF (a). Picrosirius red staining showed improved healing of the tendon-to-bone interface with a native-like densely aligned collagen structure with +GF scaffolds, compared

with the disrupted collagen structure with −GF scaffolds (b). Safranin O-stained tissue sections showed reconstruction of fibrocartilaginous interface with +GF scaffolds, reminiscent of the native state, compared with the lack of a fibrocartilaginous matrix with −GF scaffolds (c), consistentwith COL-II immunofluorescence (d). Asterisks indicate the remained scaffold structure.

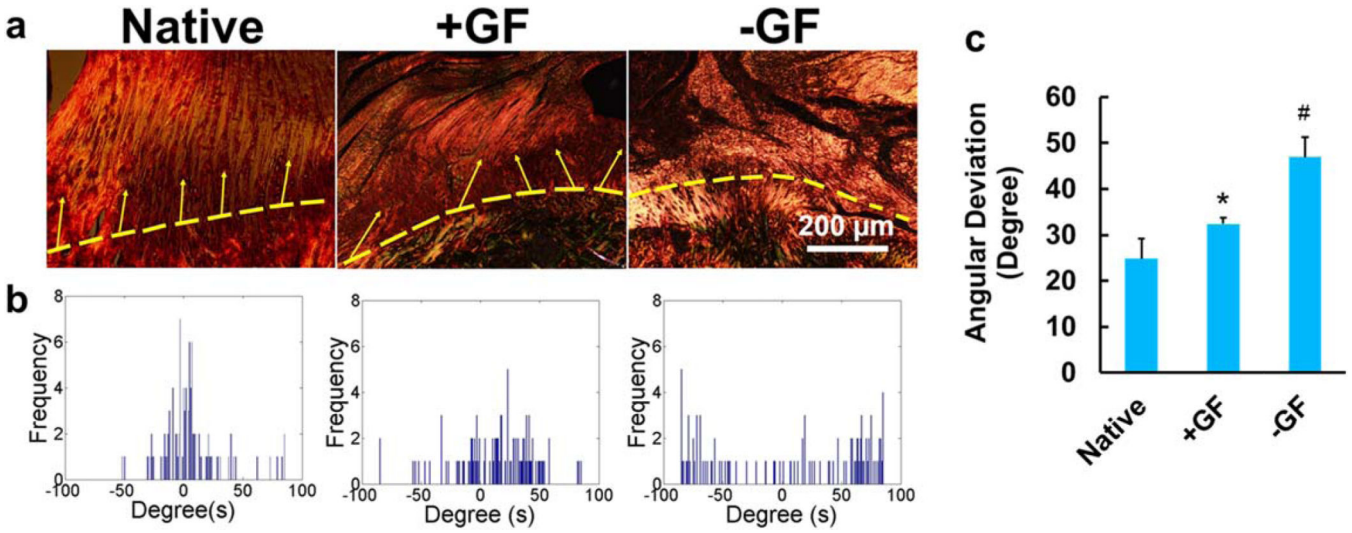

Figure 4.

Spatiotemporal GF deliveryfrom tissue engineered rotator cuff scaffolds reconstructing native-like collagen organization at the tendon-to-bone interface. Circularly polarized microscopy images show enhanced alignment of collagen fibers in +GF compared with −GF (a). Automated digital imaging processing showed a narrower angular distribution of collage fibers in native and +GF compared with −GF (b). Quantitatively, angular deviation was significantly lower in native and +GF compared with −GF (c) (error bars indicate the standard deviation: *$p < 0.05$ compared with all other groups; $n = 6$ per group).

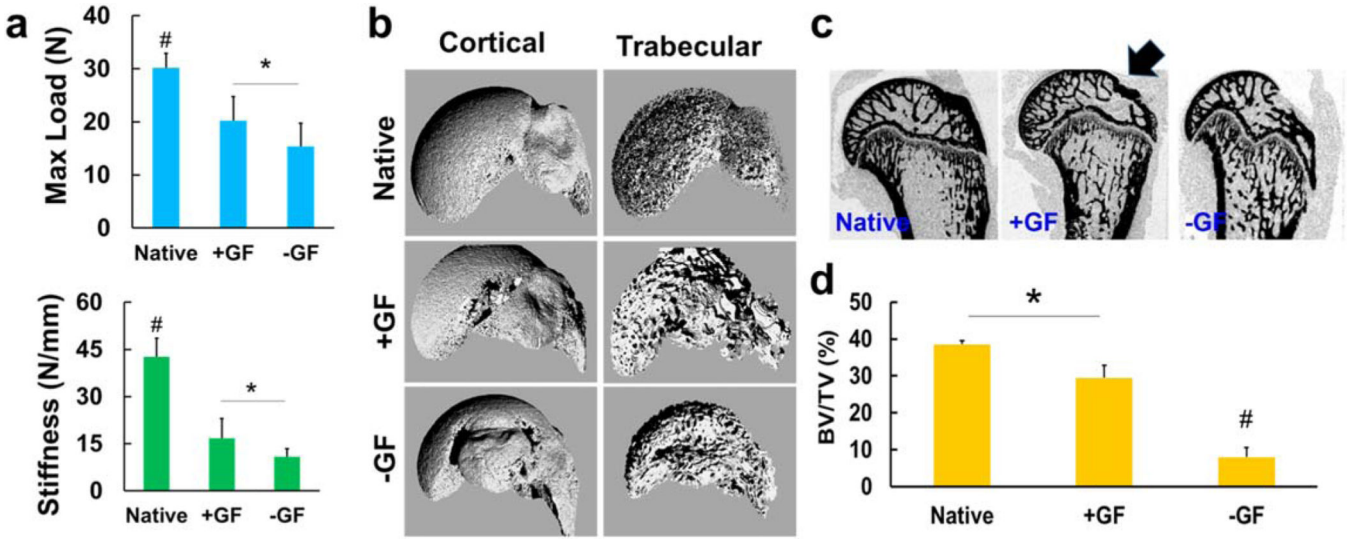

Figure 5.

Biomechanical and imaging evaluation of the regenerated supraspinatus tendon enthesis after 4 weeks of healing. The maximum tensile load and tensile stiffness in the +GF group were significantly higher than in the −GF group (a) ($n = 8$ per group; #$p < 0.05$ compared with all the groups; *$p < 0.05$). The 3D reconstructed micro-CT images of the cortical and trabecular portions of the humerus head showed visible bone loss due to the supraspinatus tendon-to-bone repair treatment (b), and images from the 2D cut-plane of micro-CT reconstruction of the proximal humerus shows an increased bone mineral portion at the tendon-to-bone repair site (arrow) in the +GF group compared with the −GF group (c). Quantitatively, the trabecular bone volume per total volume (BV/TV) was significantly higher in the +GF group than the −GF group (d) ($n = 3$ per group; *$p < 0.05$; #$p < 0.05$ compared with all other groups).

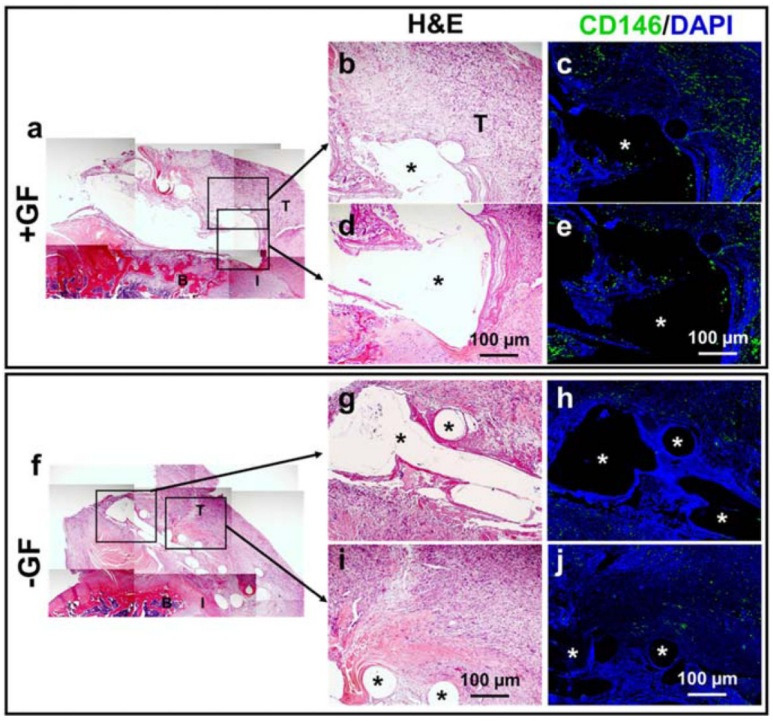

Figure 6.

Endogenous cell source for healing of the tendon-to-bone interface by GF-embedded scaffolds. One week post-operatively, implantation of scaffolds +GF resulted in abundantly more $CD146^{+}$ cells in the healing area and in the scaffolds (a)–(e) compared with −GF (f)–(j) (asterisk indicates scaffold structure) (T, tendon; B, bone, I, interface).